Microstructure-Property Relationships in a Tissue-Engineering Scaffold

Jed Johnson, Anirban Ghosh, John Lannutti

Department of Materials Science and Engineering, The Ohio State University, Columbus, Ohio 43210

Received 8 October 2006; accepted 21 November 2006
DOI 10.1002/app.25965
Published online 28 February 2007 in Wiley InterScience (www.interscience.wiley.com).

ABSTRACT: Electrospinning can produce tissue-engineering scaffolds possessing appropriate strength, biomimetic structure, economic appeal, and biocompatibility. To investigate how microstructural changes could potentially affect adherent mammalian cells, tensile samples were strained to 10, 40, and 80% extension, and adhered to double-sided carbon tape to maintain specific states of strain. While establishing the stress–strain response, we invoked polymer sintering to help verify that the ''point bonding'' concept is more significant than previously realized at both the macroscopic and microscopic length scales. Sintering successfully established the effects of deliberate, extensive point bonding/localized ''notch'' generation on mechanical properties and microstructural response without requiring chemical changes within the structure. We also found that fibers experience significant hysteresis in terms of their orientation following exposure to high values of strain. Aligned fibers provide higher strengths ($\sigma_{ave} = 2.8 \pm 0.3$ MPa vs. $\sigma_{ave} = 1.29 \pm 0.04$ MPa for unaligned fibers) but considerably lower elongation [$\varepsilon_{ave} = (30 \pm 2)\%$ vs. $\varepsilon_{ave} = (102 \pm 6)\%$]. Conversely, when strain occurs perpendicular to the aligned fiber direction total strain increases [$\varepsilon_{ave} = (188 \pm 6)\%$] while strength decreases ($\sigma_{ave} = 0.38 \pm 0.01$ MPa). Elastic response to low strains appears to estimate ultimate tensile strength. In many ways, electrospun fibers behave similarly to classic interpretations of polymer chains in that when strained in both cases elements can rearrange and translate to align along the direction of loading. J Appl Polym Sci 104: 2919–2927, 2007

Key words: biofibers; biological applications of polymers; biomaterials; biomimetic; biodegradable

INTRODUCTION

In pursuit of the general goals of tissue engineering, a variety of techniques have been developed to fabricate appropriate scaffolding. Within this range of options, it is generally agreed that electrospinning has the potential to produce scaffolds possessing the appropriate strength, nanoscalar structure, economic appeal, and biocompatibility.[1,2] The technique enjoys wide usage,[3–17] but knowledge of the mechanical response of electrospun fibers to applied stresses remains surprisingly undefined. The microstructural-level behavior of these complex electrospun structures during exposure to stress, and its potential for interaction with adherent mammalian cells, demands detailed elucidation. Although cells typically proliferate only on the outside of these structures, the behavior of cells on such surfaces may be influenced either beneficially[18–21] or, on an intuitive basis, negatively by microstructural change.

In parallel to *in vivo* applications of these electrospun scaffolds,[13,22] an enhanced understanding of how these structures respond to mechanical stresses is a critical issue. Advanced tissue-engineering applications will, in many cases, require the use of cyclic stresses[23] to develop preconditioned cellular architectures (that best simulate the properties of the target organ) without excessively damaging previously seeded cellular populations. Implantation itself will also impose basic physiological stresses that vary considerably depending on location. Because the scale of adherent cells is similar to that of electrospun fiber, basic principles of tissue formation/replacement require an improved picture of how scaffold microstructure changes in response to mechanical strain. Finally, whether or not a scaffold-plus-cells construct has the appropriate overall mechanical properties depends at least partially on structural changes within the scaffold itself.

To address these issues, we conducted a series of experiments that better establish the microstructural response of electrospun matrices to mechanical stress. The results produce a clearer picture of how these scaffolds might influence adherent mammalian cells and the breadth of such influences. We also

Correspondence to: J. Lannutti (Lannutti.1@osu.edu).
Contract grant sponsors: National Science Foundation; contract grant number: EEC-0425626.
Contract grant sponsors: NSF Integrated Graduate Education and Research Training; Ohio Oncological Biomaterials Fund.

identify the ''point bonding'' concept[24] as being more significant than previously realized and establish its effects on deformation at both the macroscopic and microscopic length scales.

EXPERIMENTAL

A 12 wt % solution of poly(ε-caprolactone) (Sigma-Aldrich, M_w = 65,000) in acetone (Mallinckrodt Chemicals) was prepared by heating acetone to 50°C followed by continuous stirring to dissolve the PCL. After cooling to room temperature, the solution was placed in a 60-cc syringe with a 20-gauge blunt tip needle and electrospun using a high voltage DC power supply (Glassman) set to 24 kV, an 18 cm tip-to-substrate distance and a 24 mL/h flow rate. A 3 × 3″ (7.6 × 7.6 cm^2) sheet ~0.5 mm in thickness was deposited onto an aluminum foil. The PCL sheets were then placed in a vacuum overnight to ensure the removal of residual acetone. High resolution ESI analysis (Esquire) was used to establish that the resulting acetone content is beneath our ability to detect it (less than 10 ppm).

Tensile dog bones with a gauge length of 20 mm and width of 2.4 mm were cut by placing the sheet between two 2-mm thick aluminum templates. A Bard-Parker #15 surgical blade was used to cut the straight edges while a 3-mm dermal punch was used to cut the radii. Great care was taken in the preparation of the gauge length to ensure that no tearing or smearing of the electrospun PCL occurred. Tensile sample thickness was measured using a digital micrometer: the gauge length of each specimen was confined between two glass microscope slides and the total thickness determined. Subtraction of the thicknesses of the individual glass slides provided the gauge length thickness. The tensile properties were determined utilizing a 1 kg load cell (model 31, Sensotec) and a strain rate of 5 mm/min on an Instron load frame (model 1322) using lightweight carbon fiber grips (A2-166 Fiber Clamp Assembly, Instron). A control group of six samples was tested initially without any exposures to establish the as-fabricated baseline ultimate tensile strength and elongation. To determine the elastic modulus, the slope of the initial linear region of each stress–strain curve was recorded.

Determination of microstructural change (or its absence) required that these samples were examined in a scanning electron microscope (XL-30 ESEM). All samples were coated with an 8-nm thick layer of osmium using an osmium plasma coater (OPC-80T, SPI Supplies, West Chester, PA). The use of osmium plasma instead of Au or Au-Pd eliminated concerns regarding PCL melting during gold-sputter coating and allowed for higher resolution imaging of the fiber surface.

To examine microstructural changes *in situ*, tensile samples were strained to 10, 40, and 80% extension and adhered to double-sided carbon tape to ''fix'' or maintain these specific states of strain. At no point during the mounting process the sample did de-adhere or cause bowing of the tape. In addition, a sample was strained to 80% elongation and was then deliberately allowed to relax (achieving zero stress) and mounted. These samples were then coated with 8 nm of osmium for viewing in the SEM as before.

Adapting the pioneering work of Inai et al.,[24] we examined the orientation of these extended fibers both visually and quantitatively. Over 100 observations per condition provided histograms showing how fiber orientation changes with strain. In addition, fiber orientation as a function of position along the length of the dog bone (positions A, B, and C in Fig. 1) was broken out of the overall data set to establish microstructural variability and general versus local alignment.

Sintering of previously electrospun fiber was carried out to establish the effects of deliberate, extensive point bonding on mechanical properties, and microstructural response. This utilized the following procedure: as-fabricated dog-bone specimens were placed into double-lined ziplock plastic bags to ensure that they remained dry. These sealed bags were then placed into a 55°C water bath for a period of 15 min after which the dog bones were removed and tested/examined as before.

For the aligned PCL fibers, a 12 wt % solution of PCL in acetone was electrospun onto a rotating mandrel 7 cm in diameter at a speed of 5000 rpm (a linear speed of 18.3 m/s). The thickness of the aligned

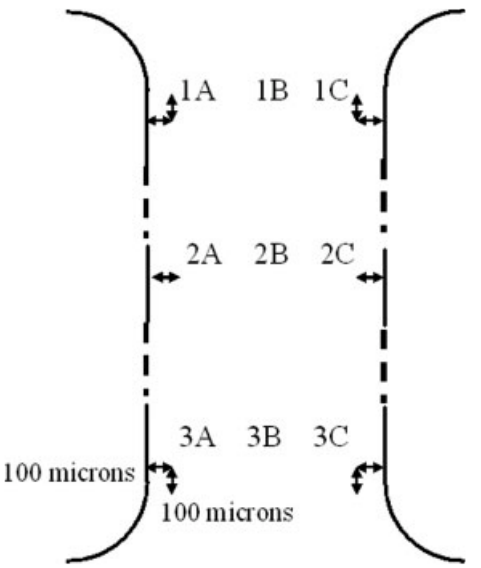

Figure 1 Schematic showing the positions A, B, and C across the gauge width and positions 1, 2, and 3 along the gauge length.

PCL samples was ~ 70 μm. Tensile dog bones were then cut in the longitudinal direction (the gauge length being parallel to the fiber alignment) and in the transverse direction (the gauge length being perpendicular to the fiber alignment).

RESULTS

All data were expressed as mean ± SE. The as-electrospun stress–strain curves for PCL without any exposure are shown in Figure 2. The average ultimate tensile strength was 1.29 ± 0.04 MPa and elongation was (102 ± 6)%. Electrospun PCL in the as-spun condition and strained to 80% elongation is compared in Figure 3. Under strain [Fig. 3(b)], considerable strain-induced fiber alignment is visible [compare to Fig. 3(a)]. Interestingly, at lower magnifications [Fig. 3(d)], the alignment is surprisingly subtle. In contrast, Figure 3(c) shows a high magnification image under this overall level of strain, suggesting a typical arrangement of crystalline and noncrystalline regions.[25]

Figure 4 gives the results of quantitative analysis of fiber orientation at 0, 10, 40, and 80% strain along with orientation remaining after unloading. The angles reported are the differences between the individual fiber axes and the loading direction; 0° is parallel and 90° is perpendicular to the load. At 0% strain, fiber orientation is clearly random (as expected); no single direction captures more than 9% of the total fiber population. At 10% strain, fiber alignment shows increases above 9% of the total population at 0° and −40° but these could conceivably be within the range of statistical error. At 40% strain, the histograms reveal an increased orientation parallel to the direction of applied force between −10° and 10°. Minima in the population oriented at 60°–70° away from the tensile axis can also be observed. The 80% strain data shows that over 60% of the fibers have now adopted positions nearly parallel to the direction of the applied stress; all other directions have less than 7% of the total.

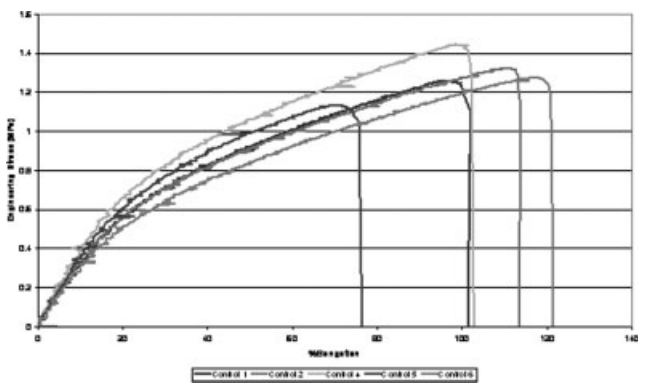

Figure 2 Stress–strain behavior of as-electrospun PCL. The average strength was 1.29 ± 0.04 MPa and elongation was (102 ± 6)%.

Following relaxation, Figure 5 shows that while the degree of alignment decreases, this overall reduction is not as dramatic as might have been anticipated. Approximately 50% of the fibers retain alignment nearly parallel to the direction of the previously applied stress (in the −10° to 10° range) and the majority of the 10% loss from this category remains within −30° to 30°. Clearly, these fibers experience significant hysteresis in terms of their orientation following the exposure to high values of strain.

Aligned fiber resulting from deposition onto the rotating mandrel is shown in Figure 6. Figure 7 shows that these fibers provide higher strengths (σ_{ave} = 2.8 ± 0.3 MPa) but considerably lower elongation [ε_{ave} = (30 ± 2)%] when strained parallel to the alignment. Fracture appears to be more gradual with evidence for fiber necking before failure. Conversely, when strain occurs perpendicular to the aligned fiber direction, final strain increases [ε_{ave} = (188 ± 6)%] while strength decreases (σ_{ave} = 0.38 ± 0.01 MPa). In the latter case, fracture is immediate and no gradual yielding is observed. The character of the data is obviously different as well; stress increases more irregularly versus strain than either the aligned or unaligned cases. The rearrangement of fibers in response to loading is manifest by the development of the cellular structure shown in Figure 8.

Figure 9 shows that in the case of sintered fibers, fracture can clearly be seen at the points of contact between aligned fibers and those crossing over them in directions not aligned with the applied stress. The resulting stress–strain behavior is shown in Figure 10. Note that the presence of these chemically bonded point contacts between individual fibers reduce tensile strength and strain to failure by 23 and 21%, respectively.

We were curious as to whether fiber alignment varied across either the width or the length of the dog-bone gauge length. As we already had data from nine different locations for each dog bone, examining this issue required only that we develop separate plots utilizing the existing data. Figure 11 compares the alignment found in locations corresponding to the edges [Fig. 11(a,c)] and middle [Fig. 11(b)] of the same dog bone at 80% elongation. As this figure illustrates, no clear trend in the data is observed; the same lack of a trend is observed regardless of location.

We then compared elastic modulus and ultimate tensile strength (Fig. 12) and found a nearly linear relationship with these particular electrospun scaffolds. For the transverse samples E = 0.40 ± 0.05 MPa; sintered E = 2.6 ± 0.3 MPa; control/as-spun

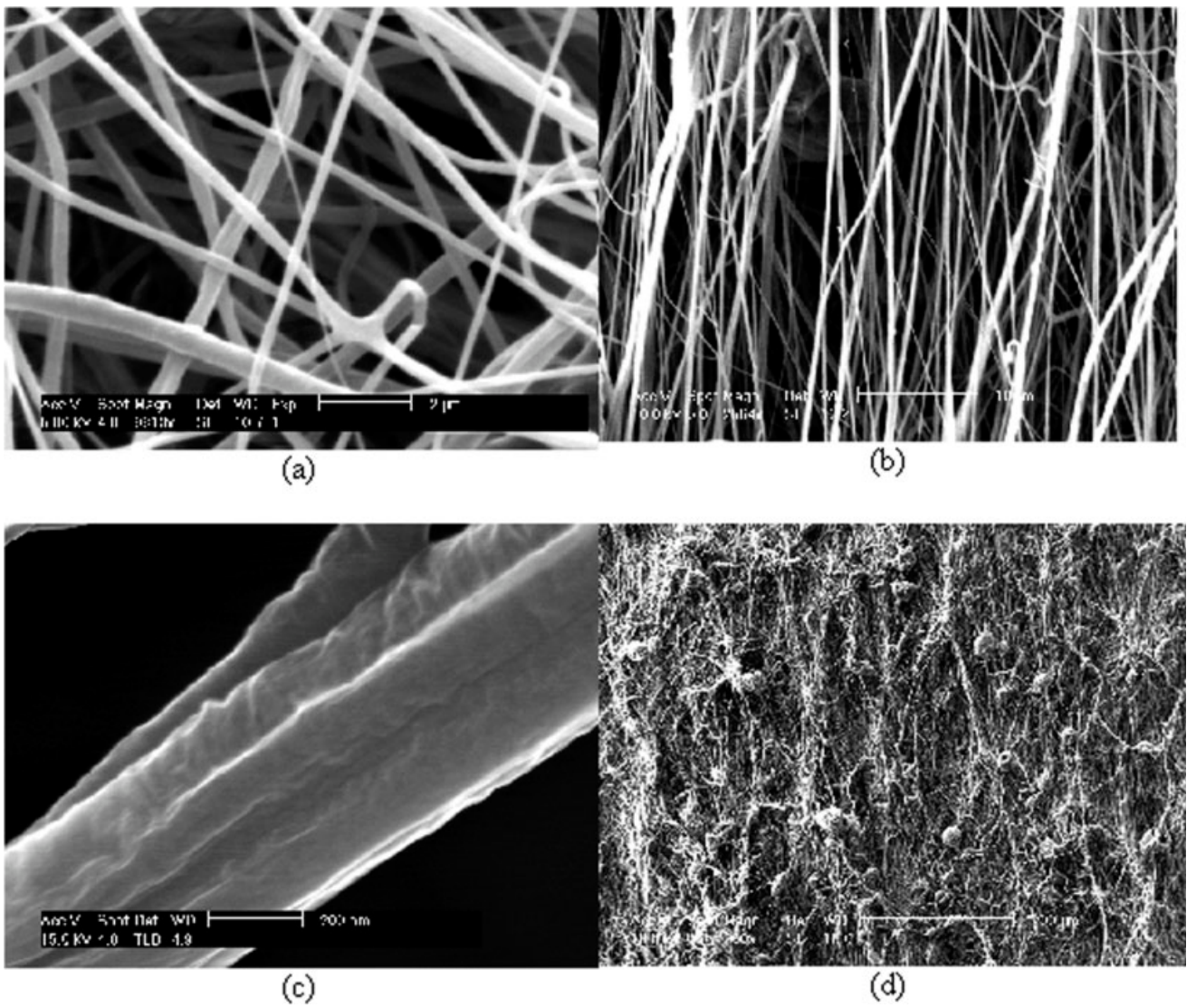

Figure 3 Electrospun PCL showing (a) the randomized nanofiber typical of the process; (b) extensive strain-induced fiber alignment on a local level *in situ* at 80% strain, (c) high magnification images revealing the surface characteristics following alignment, and (d) lower magnification images of the same set of strained fibers. Little alignment is visible in (d) although beading artifacts are obvious. In contrast with the higher magnification image found in (b) little alignment is obvious in (d).

$E = 3.3 \pm 0.2$ MPa; aligned $E = 14 \pm 2$ MPa, the error bars show that all differences in modulus are significant.

DISCUSSION

As tissue-engineering matures, a definitive description of the effects of mechanical strain on electrospun polymer scaffolds is required. Figure 4(b) shows that even strains as low as 10% appear to rearrange and align the fibers in the direction of loading. This alignment increases with the applied strain until over 60% of the fibers are aligned within $\pm 10^{\circ}$ of the direction of applied stress. If cells are present during fiber rearrangement *in vivo* or *in vitro*, they could conceivably be affected by these changes depending on the overall rate of strain. More surprising is how fiber alignment [Fig. 4(e)] is retained following a single cycle of extension and release. This has significant biological implications for a broad array of future tissue-engineering operations. As cells move across such a substrate, biased motion is likely as locomotion is based on forming and then dissolving a series of focal adhesions. Formation of these adhesions along the fiber direction must inevitably be easier than those perpendicular to that direction although this will be partially controlled by the spacing between the fibers. This has longer-term consequences for the eventual control of the architecture of tissues that develop upon such substrates.

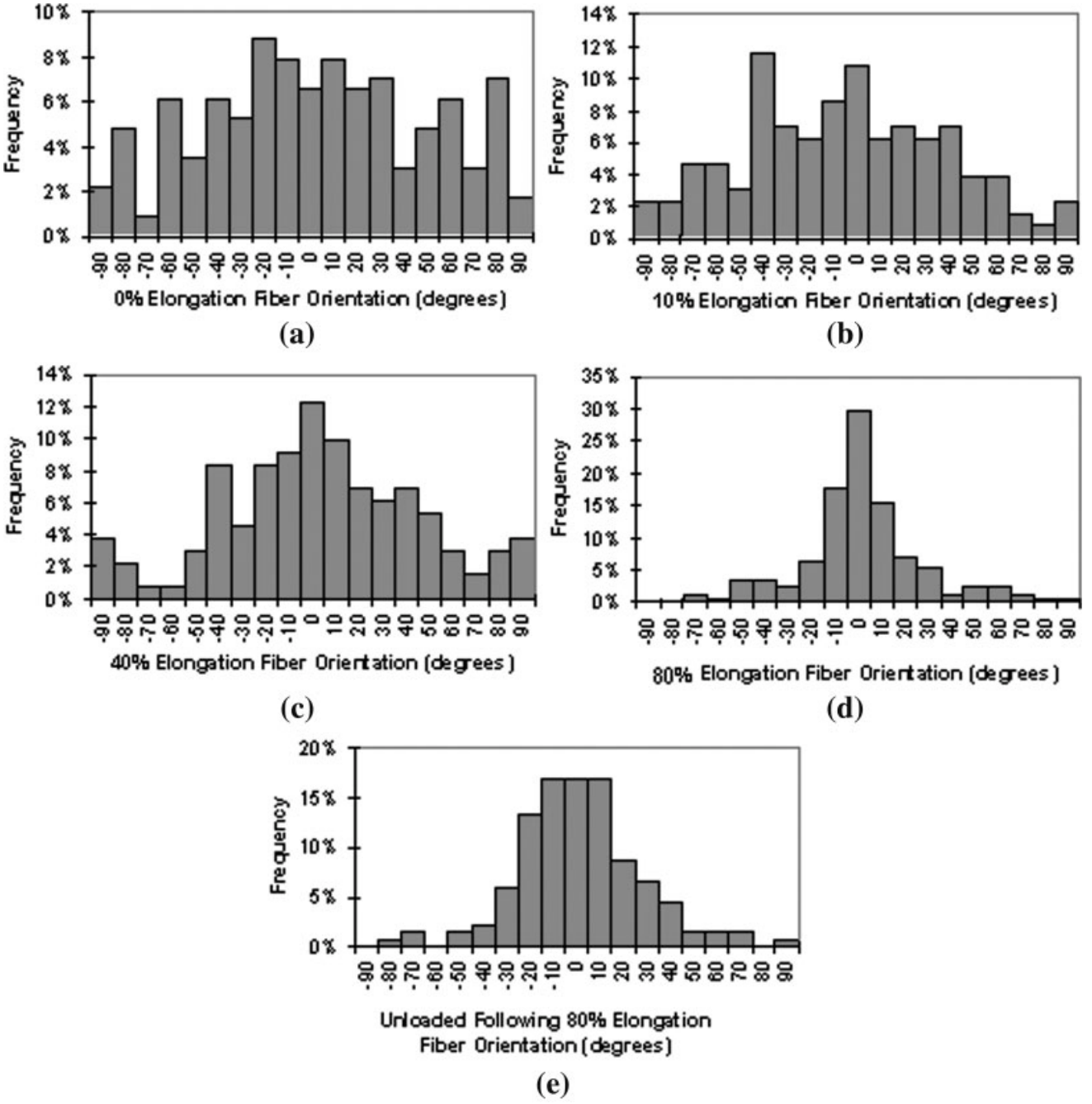

Figure 4 Quantification of fiber orientation before, during and after tensile strain: 0 (a), 10 (b), 40 (c), 80% (d), and unloaded following 80% elongation (e).

Cellular mobility parallel to the fiber direction means that one could conceivably control and direct cell proliferation and migration by prestraining scaffolds to align the fibers in certain directions. This could result in tailored structures with highly aligned fibers and, as a result, highly aligned cells.

Of additional importance is the fact that many envisioned applications of tissue-engineering scaffolds will involve the use of cyclic stresses designed to achieve specific architectures in the biological component of the developing tissue. If the scaffold experiences continuing hysteresis in which orientation increases versus the number of cycles the efficiency of the overall process will be greatly enhanced. For blood vessels, as an example, the application of cyclic pressures will produce preferential stresses that could cause significant alignment of the fibers in the circumferential direction. This could cause cellular alignment in the circumferential direction, potentially creating a more biomimetic arrangement.

Another consequence of fiber alignment either *in vitro* or *in vivo* is the associated change in elastic

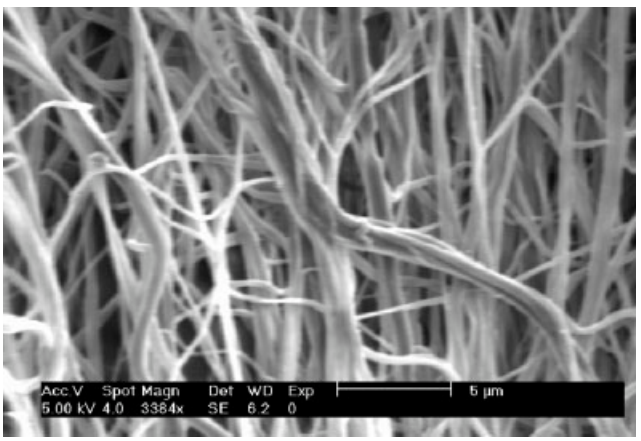

Figure 5 Image of unloaded specimen microstructure showing residual alignment following the full release of stress.

modulus. Figure 12 demonstrates that the degree of fiber alignment plays a large role in determining the modulus of the matrix. As the fibers rearrange to accommodate the applied stress to the scaffold, the directional rigidity/stiffness of the scaffold can change dramatically. An additionally useful correlation can be drawn from Figure 12 as one can clearly make relative conclusions regarding the ultimate strength at failure simply by determining the elastic response to low strains. This dependence of final UTS on initial E is particularly significant for the previously mentioned cases where low values of cyclic strain are required.

The lack of a clear trend in fiber alignment versus position within the gauge length (Fig. 11) suggests that as-spun fiber meshes at these particular length scales are able to efficiently distribute load to avoid edge effects. A concern was the presence of cut fiber at the sample edges, which would act to relieve stress by allowing interfiber translation. If this effect

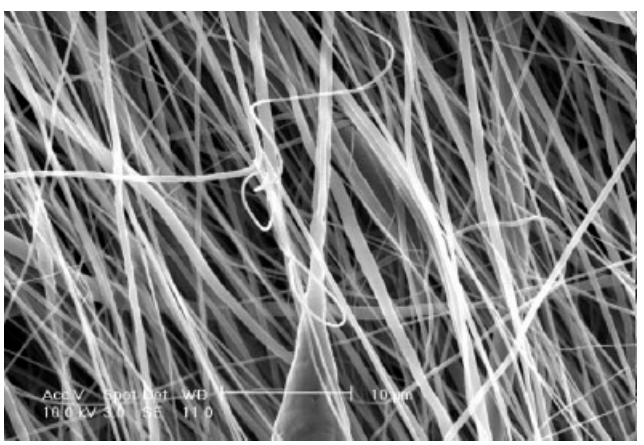

Figure 6 PCL fiber deposited on a 7-cm diameter mandrel rotating at 18.3 m/s to achieve alignment of fibers.

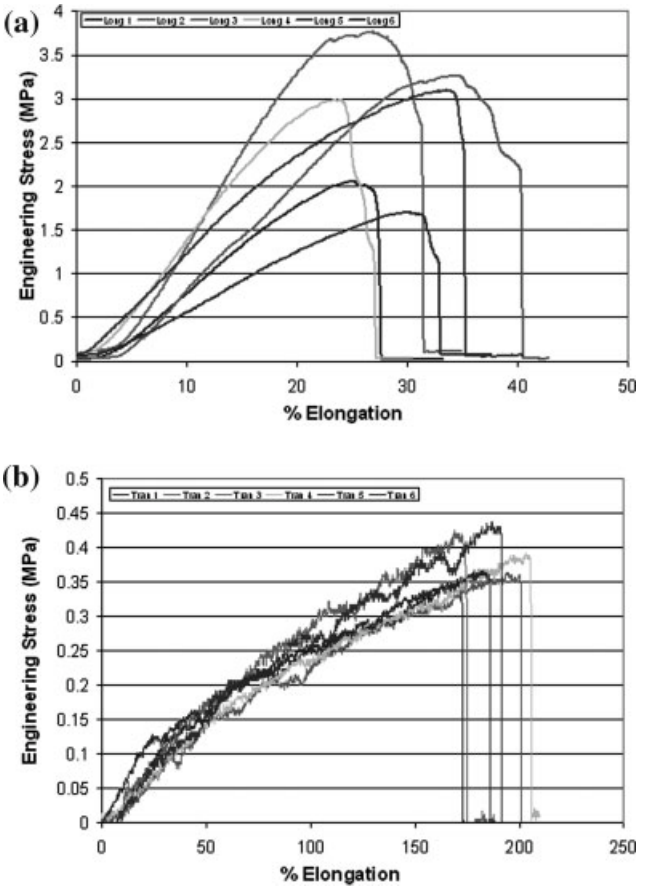

Figure 7 Aligned electrospun fiber tested in the (a) parallel and (b) transverse directions.

was substantial, one would expect to see significantly higher alignment in the edge positions A and C versus the middle of the gauge width (position B). Figure 11 shows no significant differences between the edge and middle positions. Edge effects may be

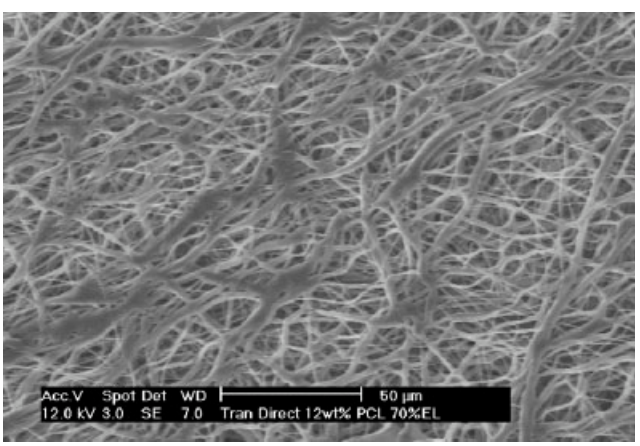

Figure 8 Transverse tensile sample strained to 70% showing a cellular arrangement of fibers. Fibers were originally aligned in a specific direction (solid arrow) before perpendicular strain (dashed arrow) was applied.

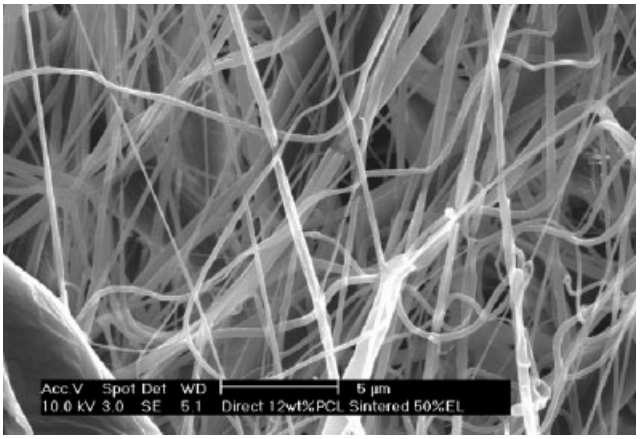

Figure 9 SEM of PCL sintered at 55°C for 15 min then strained (in the vertical direction) to 50%. Careful examination reveals multiple points of fiber failure occurring at the intersections between locally aligned and unaligned fibers.

present in considerably wider specimens as the interior fibers become further isolated from the free edges. For the moment, the accommodation of strain in this microstructure appears to be relatively global at these particular levels of strain and overall strain rate.

We used a mandrel rotating at a linear speed of 18.3 m/s to achieve the reasonably parallel fibers shown in Figure 6. Mathew et al.[26] examined electrospun PBT produced on a mandrel rotating at a similar maximum speed. Although no microstructural characterization of the as-strained material was provided, they also observe a fourfold increase in strength in the direction of alignment and a similar decrease in strength perpendicular to that axis. In contrast, Ayres et al.[27] show an inconclusive trend of strength parallel versus perpendicular to the axis of rotation for collagen fibers spun using a variety of solids concentrations.

By testing in both the longitudinal and transverse directions, we gained significant insight into the

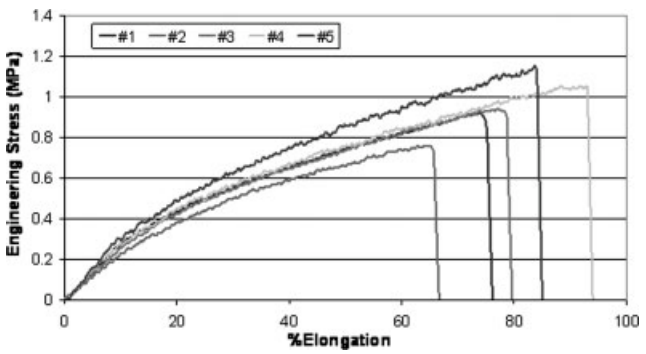

Figure 10 Stress–strain behavior of point-bonded microstructure following sintering at 55°C for 15 min.

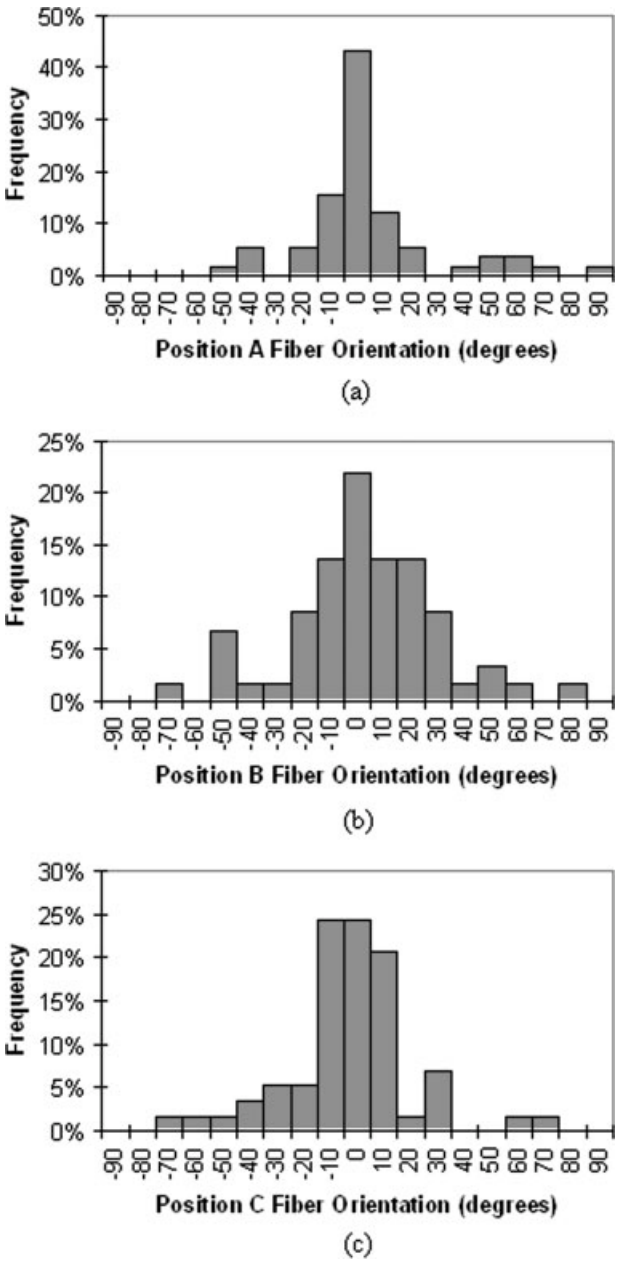

Figure 11 Quantification of fiber orientation versus position (a, b, and c, see Fig. 1) showing variable fiber alignment across the gauge width at 80% elongation.

mechanisms of strain and failure. In Figure 7(a), orientation along the axis of strain leads to transfer of load to the fibers causing a gradual yielding process that result from necking of individual fibers at many points in the microstructure followed by total failure. Conversely, the transverse direction samples yield by extensive fiber rearrangement reflected in the ragged nature of the stress–strain curve [Fig. 7(b)]. The quantitative behaviors are reasonable in light of the alignment shown in Figure 4: pre-existing alignment makes additional alignment more difficult (decreasing total strain) while increasing the allowed

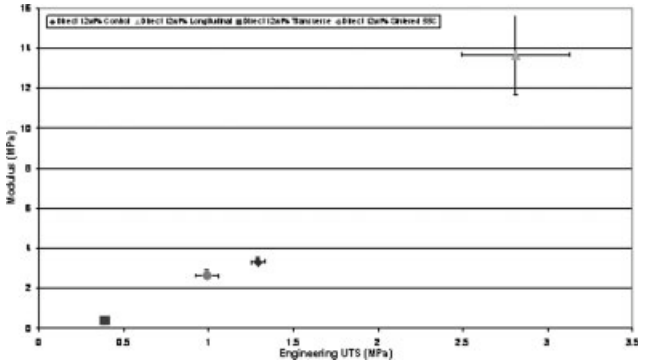

Figure 12 Comparison showing a nearly linear relationship between elastic modulus and ultimate tensile strength.

load as fibers are more able to carry the load directly rather than through interfiber interactions/rearrangement. Strain transverse to the direction of alignment results in an increase of 84% in elongation because of the realignment of initially aligned fibers into a cellular structure (Fig. 8) and a decrease of 71% in strength as fewer fibers are able to bear load efficiently and weak interfiber interactions are relatively dominant.

The behavior we observe is qualitatively similar to that observed elsewhere for unoriented, unbonded nanofiber.[28] Previously, randomly deposited fibers [Fig. 3(a)] are heavily aligned along the direction of loading. In Figure 3(b), the 80% strained sample shows (at higher magnifications) considerable alignment along the axis of strain.

In this context, Figure 4 shows that a gauge length consisting of electrospun fiber obviously undergoes different levels of orientation depending on stress. Figure 11 suggests that as some areas undergo alignment, additional stress is efficiently transferred to relatively unstrained areas, distributing the load evenly throughout the gauge length.

The effects of intersection or bonding points on mechanical properties could easily obscure differences in fiber orientation. A true ''web'' of highly interconnected nanofibers would be expected to undergo very limited relative nanofiber translations. In addition, these point bonds act as stress-concentrating notches leading to the localized fiber failure observed in Figure 9. This explains the immediate transition to end-stage deformation/fully linear behavior observed in the literature[29–32] when obvious point bonding exists. In these cases, no nonlinear ''knee'' occurs in the stress–strain curve and extension is completely linear as demonstrated in the work of Hansen et al.[32] There, ''wet'' fiber followed the dry fiber curve although fracture occurred at substantially lower strains. Those familiar with such structures will recall that determining the presence or absence of interfiber bonding in the SEM can be challenging: if only point contacts exist (rather than obvious fiber intersections), the structure looks much the same as unbonded nanofiber. He et al. observed a high, almost vertical, initial slope followed by a fully linear regime until fracture.[31] Given that their nanofibers were both (1) collagen coated and (2) showed extensive point bonding, it seems likely that this behavior is because of the initial strain and fracture of an array of ''stiff'' point bonds[33] consisting purely of collagen followed by strain of the remaining not-point-bonded matrix.

Given the obvious differences between what we observed versus the work of He et al., we were curious as to why the tensile deformation of electrospun materials is sometimes linear and other times nonlinear. Recently, enough test data has emerged to allow for direct comparisons of the mechanical behavior of different systems. Although similar aspects of the orientation in Figure 3(b) have been observed,[24,29] none has been as pronounced. The interest in the relative behavior of point-bonded versus not-point-bonded structures formed the driving force for our work involving sintered microstructures of electrospun fibers. PCL has a low melting point (60°C) that allows for easy, reproducible structural modification. In an ideal sense, sintering also allows for us to largely preserve the original structure consisting of discrete fibers while introducing extensive interfiber point-bonding, a change that would be very difficult to achieve via electrospinning alone. You et al.[34] used a ''thermal bonding'' exposure involving temperatures well above T_m for their system (PLA). The shrinkage involved was ~75%; in our system, shrinkage was negligible and the thermal exposure was well below the melting point, producing the limited bonding characteristic of true sintering. You et al.[34] show an initial fiber structure that is heavily bonded probably because of a small source-substrate distance. As a result, their SEM data suggest that their more aggressive thermal treatments transform an initial weblike structure into a much more heavily bonded weblike structure displaying a simultaneous increase in strength and final elongation.

Some have concluded that pre-existing molecular orientation in these fibers leads to reduction in the elongation to failure.[29] Although this ''strain-hardening'' argument may hold for heavily point-bonded structures in which load may be shared relatively equally, in less- or fully unbonded structures elongation to failure is clearly accommodated by the rearrangement of less-well oriented fibers. Specific fiber anisotropies in the as-deposited fibers strongly influence both microstructural and macroscopic response to mechanical deformation.

Perhaps appropriate to the reduced values of scale associated with what are often referred to as polymer ''nanofibers,'' we see considerable overlap between the components of basic, classic explanations of thermoplastic polymer chain behavior, and the behavior of electrospun fiber:

1. Alignment of elements in the direction of strain.
2. Unaligned elements held together by physical (overlap, entanglement) and weak frictional interactions.
3. Translation between elements allowing permanent macroscopic deformation.

Like secondary bonding concepts, in polymer chains electrospun fibers, when strained, rearrange and translate to align along the direction of loading.

This view of electrospun fiber deformation is obviously informed by standard crazing phenomena in which fibrils containing well-oriented polymer chains form. Unoriented polymer chains in the vicinity either collapse or are eventually oriented and added to the fibrils. Electrospun polymer fibers appear to follow an identical hierarchy of rearrangement driven by the applied macroscopic stress. Recently, Tan et al.[35] used AFM to demonstrate that the tensile behavior of individual electrospun PEO fibers was essentially equal to that of the bulk. In all cases reported in the literature to date, assemblies of electrospun fiber are found to be far weaker than their bulk counterparts. Issues related to fiber rearrangement and early failure are clearly the cause of this discrepancy.

CONCLUSIONS

The strain and failure mechanisms of electrospun PCL involve the rearrangement and alignment of substantial fractions of individual nanofibers. These substantial changes could have considerable effects on the form and viability of any adherent/interpenetrating cells and the resulting strength of the nanofiber matrix. Dramatic microstructural change in strained nanofibers would likely rearrange, loosen or even eliminate contacts between nanofibers, and adherent cells. This concept becomes critical in predicting and understanding the physical and biological performance of cell–tissue constructs as they undergo strain either *in vivo* or *in vitro*.

Any opinions, findings, and conclusions or recommendations expressed in this material are those of the authors and do not necessarily reflect the views of the National Science Foundation. We express our deepest thanks to Darrell Reneker of the University of Akron for his comments and support.

References

1. Pham, Q. P.; Sharma, U.; Mikos, A. G. Tissue Eng 2006, 12, 1197.
2. Lannutti, J.; Reneker, D.; Ma, T.; Tomasko, D.; Farson, D. Mater Sci Eng C, to appear.
3. Li, W. J.; Tuli, R.; Huang, X. X.; Laquerriere, P.; Tuan, R. S. Biomaterials 2005, 26, 5158.
4. Fujihara, K.; Kotaki, M.; Ramakrishna, S. Biomaterials 2005, 26, 4139.
5. Kwon, I. K.; Kidoaki, S.; Matsuda, T. Biomaterials 2005, 26, 3929.
6. Zeng, J.; Chen, X. S.; Liang, Q. Z.; Xu, X. L.; Jing, X. B. Macromol Biosci 2004, 4, 1118.
7. Khil, M. S.; Bhattarai, S. R.; Kim, H. Y.; Kim, S. Z.; Lee, K. H. J Biomed Mater Res Part B: Appl Biomater 2005, 72, 117.
8. Zhang, Y. Z.; Ouyang, H. W.; Lim, C. T.; Ramakrishna, S.; Huang, Z. M. J Biomed Mater Res Part B: Appl Biomater 2005, 72, 156.
9. Li, W. J.; Tuli, R.; Okafor, C.; Derfoul, A.; Danielson, K. G.; Hall, D. J.; Tuan, R. S. Biomaterials 2005, 26, 599.
10. Hsu, C. M.; Shivkumar, S. J Mater Sci 2004, 39, 3003.
11. Hsu, C. M.; Shivkumar, S. Macromol Mater Eng 2004, 289, 334.
12. Shin, M.; Ishii, O.; Sueda, T.; Vacanti, J. P. Biomaterials 2004, 25, 3717.
13. Shin, M.; Yoshimoto, H.; Vacanti, J. P. Tissue Eng 2004, 10, 33.
14. Li, W. J.; Danielson, K. G.; Alexander, P. G.; Tuan, R. S. J Biomed Mater Res A 2003, 67, 1105.
15. Zeng, J.; Chen, X. S.; Xu, X. Y.; Liang, Q. Z.; Bian, X. C.; Yang, L. X.; Jing, X. B. J Appl Polym Sci 2003, 89, 1085.
16. Yoshimoto, H.; Shin, Y. M.; Terai, H.; Vacanti, J. P. Biomaterials 2003, 24, 2077.
17. Lee, K. H.; Kim, H. Y.; Khil, M. S.; Ra, Y. M.; Lee, D. R. Polymer 2003, 44, 1287.
18. Agarwal, S.; Deschner, J.; Long, P.; Verma, A.; Hofman, C.; Evans, C. H.; Piesc, N. Arthritis Rheum 2004, 50, 3541.
19. Deschner, J.; Hofman, C. R.; Piesco, N. P.; Agarwal, S. Curr Opin Clin Nutr Metab Care 2003, 6, 289.
20. Long, P.; Gassner, R.; Agarwal, S. Arthritis Rheum 2001, 44, 2311.
21. Deschner, J.; Perera, P.; Wang, Z.; Lannutti, J.; Agarwal, S. Tissue Eng 2006, 12, 998.
22. Annis, D.; Bornat, A.; Edwards, R. O.; Higham, A.; Loveday, B.; Wilson, J. Trans Am Soc Artif Intern Organs 1978, 24, 209.
23. Shin, H. J.; Lee, C. H.; Cho, I. H.; Kim, Y. J.; Lee, Y. J.; Kim, I. A.; Park, K. D.; Yui, N.; Shin, J. W. J Biomater Sci Polym Ed 2006, 17, 103.
24. Inai, R.; Kotaki, M.; Ramakrishna, S. J Polym Sci Part B: Polym Phys 2005, 43, 3205.
25. Cicero, J. A.; Dorgan, J. R. J Polym Environ 2001, 9, 1.
26. Mathew, G.; Hong, J. P.; Rhee, J. M.; Leo, D. J.; Nah, C. J Appl Polym Sci 2006, 101, 2017.
27. Ayres, C.; Bowlin, G. L.; Henderson, S. C.; Taylor, L.; Shultz, J.; Alexander, J.; Telemeco, T. A.; Simpson, D. G. Biomaterials 2006, 27, 5524.
28. Zhao, Z. Z.; Li, J. Q.; Yuan, X. Y.; Li, X.; Zhang, Y. Y.; Sheng, J. J Appl Polym Sci 2005, 97, 466.
29. Pedicini, A.; Farris, R. J. Polymer 2003, 44, 6857.
30. Lee, K. H.; Kim, H. Y.; Ryu, Y. J.; Kim, K. W.; Choi, S. W. J Polym Sci Part B: Polym Phys 2003, 41, 1256.
31. He, W.; Ma, Z. W.; Yong, T.; Teo, W. E.; Ramakrishna, S. Biomaterials 2005, 26, 7606.
32. Hansen, L. M.; Smith, D. J.; Reneker, D. H.; Kataphinan, W. J Appl Polym Sci 2005, 95, 427.
33. Huang, Z. M.; Zhang, Y. Z.; Ramakrishna, S. J Polym Sci Part B: Polym Phys 2005, 43, 2852.
34. You, Y.; Lee, S. W.; Lee, S. J.; Park, W. H. Mater Lett 2006, 60, 1331.
35. Tan, E. P. S.; Goh, C. N.; Sow, C. H.; Lim, C. T. Appl Phys Lett 2005, 86, 073115.